J Mater Sci (2009) 44:5654–5661
DOI 10.1007/s10853-009-3796-x

Effect of combining plane-strain compression with equal channel angular pressing on mechanical properties and texture development in an Al alloy

Abdulhakim A. Almajid · Ehab A. El-Danaf · Mahmoud S. Soliman

Received: 3 June 2009 / Accepted: 5 August 2009 / Published online: 18 August 2009

Abstract Commercial purity aluminum (1050) was processed via equal channel angular pressing (ECAP) to one, two, and four passes using route B_c in a 90° channel die, and subsequently compressed in plane strain in two different loading directions, and to two different strain levels. One of the plane-strain-loading directions is parallel to the ECAP forward direction, while the other is perpendicular to it. The flow response in plane-strain compression of the ECAP processed samples revealed an anisotropic behavior, one loading direction systematically gave higher flow stresses. A strain path change parameter was calculated for the two deformation schemes, to justify this anisotropic behavior. Texture evolution, of the plane-strain-compressed samples, was measured, and a transition to the rolling texture was always evidenced. The evolution of the main ideal rolling-texture components obtained from such a combination of deformation schemes, ECAP and plane-strain compression, is presented.

Introduction

Equal channel angular pressing (ECAP) is becoming a potential and innovative processing technique for the production of ultra fine grained (UFG) structure in bulk materials. A recent investigation [1], using electron back scattered diffraction (EBSD), on the microstructure evolution (cell size and misorientation angle) in commercially pure aluminum 1050 processed by ECAP to 16 passes, has shown that grains break up into cell structure that reduces gradually in size with number of ECAP passes and attains an average value of 0.6 μm in the face plane (normal to the extrusion direction) and 0.85 μm in the flow plane (parallel to the extrusion direction), and that the misorientation angle has developed to about 27°, after the 16th pass. The development of UFG structures was carried out through studying different ECAP parameters (die channel angle, number of pressings, processing route or in other words billet rotation between passes, relief angles in the die, back pressure, friction, pressing speeds, and ECAP processing temperature) [2–4]. Berbon et al. [5] have investigated the influence of pressing speed in ECAP using samples of pure Al with a range of pressing speeds from 0.6 to 600 mm/min. Their results showed that the speed of pressing had no significant influence on the equilibrium grain size. However, it was shown that the nature of the microstructure is dependent on the pressing speed, because recovery occurs more easily at the slower speeds, so that the microstructure is then more equilibrated. This implies that, though there is no effect on the grain size of the refined structure, texture could still be affected due to the change of dynamic recovery rates.

The shearing characteristics of the ECAP samples, pressed through consecutive passes, may be changed by rotating the sample between each pass. The microstructure and texture developed in the ECAP samples are greatly influenced by the processing route [6]. ECAP was found to be an effective technique to control texture strength and crystallographic orientations. Compared to conventional techniques, ECAP offers a large variety of parameters for controlling texture, of which the most obvious are the number of passes and the processing route, due to the frequent strain path changes (SPCs) and severe plastic

A. A. Almajid · E. A. El-Danaf (✉) · M. S. Soliman
Mechanical Engineering Department, Center of Excellence for Research in Engineering Materials, College of Engineering, King Saud University, P.O. Box 800, Riyadh 11421, Saudi Arabia
e-mail: edanaf@ksu.edu.sa

deformation involved. These differences in crystallographic textures can have a great impact on the processed sheet mechanical properties and formability [7].

Saiyi et al. [8] have measured the texture developed in one pass in aluminum and demonstrated that these ECAP texture orientations can be derived from those for negative simple shear, by increasing the ϕ_1 of simple shear ideal orientations by 45°, which is the angle that transforms the shear reference system $X'Y'Z'$ to the billet axes system XYZ in a 90° channel ECAP die, while the other two euler angles remain the same (refer Fig. 1; where an ECAP processed billet is displayed and the two sets of axes are shown). These orientations distribute along two partial fibers, similar to the development of $\{111\}\ \langle uvw\rangle$ and $\{hkl\}\ \langle 110\rangle$ partial fibers in simple shear deformation of fcc materials. The two partial fibers that constitute the texture orientations after 1 ECAP pass are designated $\{111\}_\theta\ \langle uvw\rangle$ with a $\{111\}$-plane counter clockwise rotated (CCW) by 45° about the Z axis toward the Y' axis and the other designated as $\{hkl\}\ \langle 110\rangle_\theta$ with a $\langle 110\rangle$-direction CCW rotated by 45° about the Z axis toward the X' axis. Numerous studies [9–11], in the last 4 years, focused on finite element modeling and simulation of the ECAP process and the use of crystal plasticity theory codes to predict texture. This study was carried out in the flow plane either in the shear reference axes system ($X'Y'$) (see Fig. 1) [9], where the deformation gradient tensor was written for simple shear along—X' accordingly, or in the billet reference axes system (XY) (see Fig. 1) [10] where the gradient tensor was transformed to the billet axes system by a 45° clockwise rotation. Other study was carried out on texture prediction out of the flow plane; YZ plane (see Fig. 1) [11], and ascertained that the initial texture before ECAP plays a key role in the formation of the final texture.

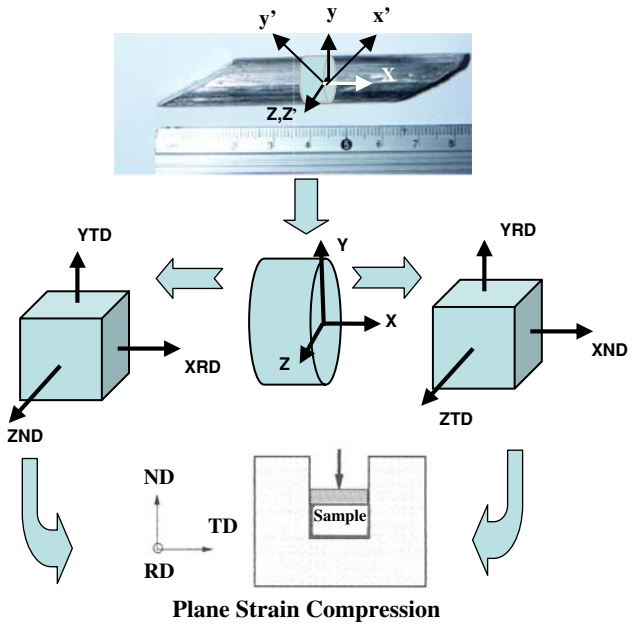

Fig. 1 A sketch showing the sequence of deformation after ECAP processing

The texture development of cold-rolled fcc metals can best be described by orientation concentrations along two fibers, the α fiber ($\langle 110\rangle$ parallel to the sheet normal) and the β fiber ($\langle 110\rangle$ tilted 60° toward the rolling direction). These are usually called skeleton lines, which are mainly determined by connecting the density maxima in the different orientation distribution function (ODF) sections. The density along these lines has been repeatedly discussed in the literature [12, 13]. The α fiber extends from the Goss (G) orientation $\{011\}\ \langle 100\rangle$ to the $\{011\}\ \langle 21\bar{1}\rangle$ B orientation (brass component). The β fiber extends through three main components $\{112\}\ \langle 21\bar{1}\rangle$, $\{123\}\ \langle 63\bar{4}\rangle$, and $\{011\}\ \langle 21\bar{1}\rangle$ which are referred to as Cu (copper), S, and B (brass) orientations, respectively. The texture of different fcc alloys differ mainly in the volume fractions of these components.

While the texture that develops in ECAP and plane-strain compression is individually well studied, the texture that could evolve when the two deformation paths are combined has not been systematically studied. The texture of plane-strain-compressed samples that were previously subjected to one, two, and four ECAP passes, via route B_c will be investigated. The loading in plane-strain compression will be conducted in two different directions. Our focus is directed toward combining ECAP and plane-strain compression to investigate the texture evolution resulting from such combined processes, for 1050 aluminum alloy which is characterized as a high stacking fault energy material, and is known to develop a copper-type texture upon rolling. Manipulating the deformation path for possible development of a brass-type texture or balanced brass- and copper-texture components, in such a high stacking fault energy material, will be investigated. In addition, the true stress–true strain response obtained in plane-strain compression of the ECAP processed specimens will be presented.

Experimental procedure

Cylindrical samples of commercial purity 1050 aluminum of 12 mm in diameter were machined from cold-rolled plate then subsequently annealed at 600 °C for 8 h to yield an average grain size of 600 μm. These samples were ECAP processed in a 90° channel die with $\Psi = 0$, via route B_c, the samples were rotated in the same sense by 90° between each pass. The number of passes used was one, two, and four. The pressing was conducted at a speed of 10 mm/min. Disks of about 8 mm in thickness were cut

from the ECAP processed samples as seen in Fig. 1, and then further machined to produce an almost cubic sample of sides of about 8 mm. These cubic samples were inserted into another die that applied plane strain. The surfaces were carefully marked so that the two loading directions during plane-strain compression were identified and are termed here as XND and ZND (see Fig. 1). Plane-strain compression tests were performed using an Instron machine with a constant speed of 0.5 mm/min. Teflon sheet and high pressure grease were used to nearly isolate the effect of friction.

Crystallographic textures were obtained using a Schimadzu X7000 diffractometer, using Cu-k_α radiation. Texture was investigated along the mid-thickness plane for all samples for consistency; this was done to insure capturing the rolling texture and to eliminate the effect of friction on texture which is maximized at the top and bottom surface. All samples, for X-ray diffraction, were mechanically ground to 1000 grit size paper and mechanically polished using 3- and 1-μm alumina paste. The (100), (110), and (111) pole figures were measured. The raw data were corrected for background and defocusing using a correction file generated from an aluminum sample with a random texture. Recalculated pole figures and ODF plots were generated by the iterative series expansion method with a maximum order of 22, which gives the volume fraction of grains oriented along a certain ideal orientation defined with Euler angles representation (ϕ_1 ϕ ϕ_2) in Bunge's notation. However, because of the cubic crystal symmetry of aluminum alloys, and because of the specimen symmetry in rolling, it is possible to reduce the angular range to $0° \leq \phi_1 \leq 90°$, $0° \leq \phi \leq 90°$, $0° \leq \phi_2 \leq 90°$ in which each orientation occurs at least once.

Results and discussion

Stress–strain response

Figure 2a, b, and c represents the true axial stress versus the true axial strain obtained in plane-strain compression for samples that were ECAP processed to one, two, and four passes, respectively. In both the cases (XND and ZND) the stress–strain is characterized by an initial transient hardening stage followed by almost perfect plastic behavior, and especially for ZND where slight strain softening can be observed. It is concluded from the figure that ZND has a consistently higher flow stress that could be related to the SPC from ECAP to the respective subsequent deformation modes. The softening behavior during the deformation process was recently reported by Terada et al. [14] in UFG aluminum produced by accumulative roll bonding. This finding can be interpreted and understood on

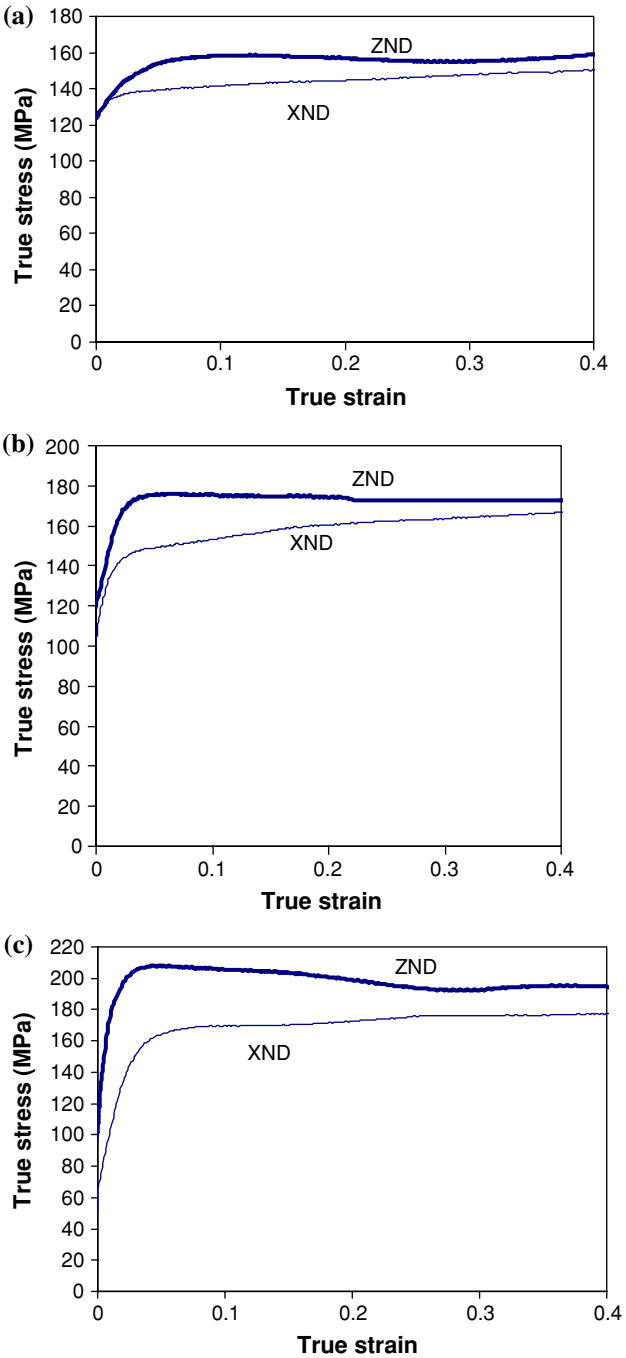

Fig. 2 True axial stress versus true axial strain, for samples ECAP processed to one (**a**), two (**b**), and four (**c**) passes and plane strain compressed in XND and ZND

the basis of the SPC parameter, termed as θ, which was originally proposed by Schmitt et al. [15], and recently by Li [16]. The SPC during a two-stage deformation sequence can be measured by considering the directionalities of the strain or strain rate tensors associated with the two monotonic deformations. Let $\dot{\varepsilon}^{(1)}$ and $\dot{\varepsilon}^{(2)}$ be the strain rate tensors associated with the first and second deformation

stages, respectively. Then an SPC parameter, can be calculated as the scalar product of the two tensors expressed in the same reference frame

$$\theta = \mathrm{Cos}\alpha = A^{(1)}{:}A^{(2)} = \frac{\dot{\varepsilon}^{(1)}}{\sqrt{\dot{\varepsilon}^{(1)}{:}\dot{\varepsilon}^{(1)}}}{:}\frac{\dot{\varepsilon}^{(2)}}{\sqrt{\dot{\varepsilon}^{(2)}{:}\dot{\varepsilon}^{(2)}}} \quad (1)$$

where $A^{(1)}$ and $A^{(2)}$ are the unit vectors in the strain rate space associated with $\dot{\varepsilon}^{(1)}$ and $\dot{\varepsilon}^{(2)}$, respectively. The SPC parameter, for ECAP followed by plane-strain compression with X being the loading direction, Y is the rolling direction, and Z is the transverse direction, can be calculated using the appropriate strain rate equations as follows:

$$\dot{\varepsilon}^{(2)}_{xyz} = \begin{pmatrix} \dot{\varepsilon}^{(2)}_x & 0 & 0 \\ 0 & \dot{\varepsilon}^{(2)}_y & 0 \\ 0 & 0 & 0 \end{pmatrix} \quad (2)$$

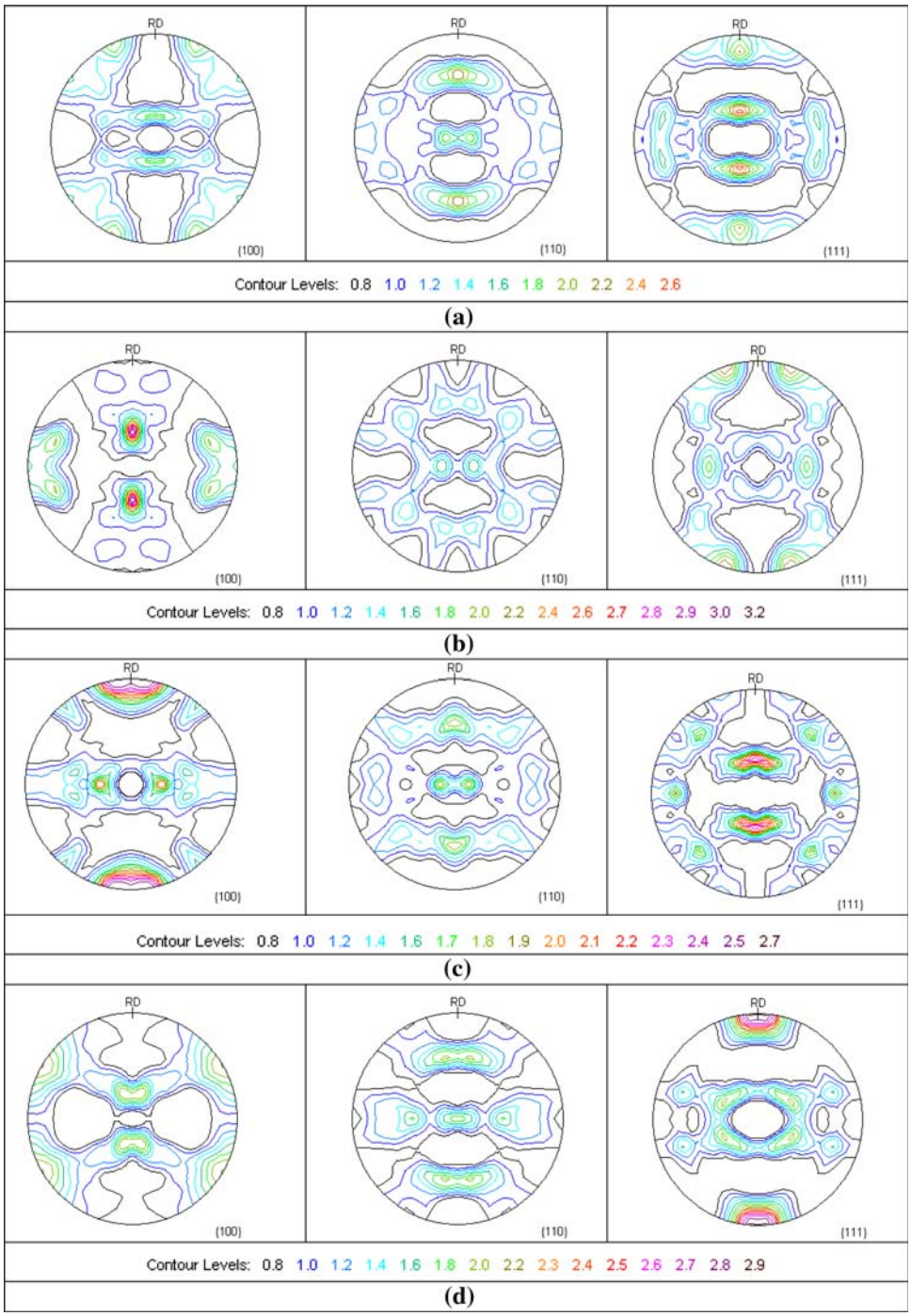

Fig. 3 (100), (110), and (111) pole figures for the sample ECAP processed to four passes and further plane strain compressed to a true axial strain of 0.5 via XND (**a**) and ZND (**b**). XND (**c**) and ZND (**d**) represent pole figures for same ECAP condition, but the plane-strain compression was to a true axial strain of 1.0

This brings $A^{(2)}$ to be:

$$A^{(2)}_{xyz} = \frac{1}{\sqrt{\left(\dot{\varepsilon}^{(2)}_x\right)^2 + \left(\dot{\varepsilon}^{(2)}_y\right)^2}} \begin{pmatrix} \dot{\varepsilon}^{(2)}_x & 0 & 0 \\ 0 & \dot{\varepsilon}^{(2)}_y & 0 \\ 0 & 0 & 0 \end{pmatrix} \quad (3)$$

By taking $A^{(1)}$ (considering ECAP being the first stage of deformation) as reported by Saiyi [16], the value of θ was calculated to be:

$$\theta = \frac{\dot{\varepsilon}^{(2)}_x - \dot{\varepsilon}^{(2)}_y}{\sqrt{2\left[\left(\dot{\varepsilon}^{(2)}_x\right)^2 + \left(\dot{\varepsilon}^{(2)}_y\right)^2\right]}} \quad (4)$$

Adapting Eq. 4 to plane-strain compression with X being the loading direction, we have $\dot{\varepsilon}_z = 0$, $\dot{\varepsilon}_x = -\dot{\varepsilon}$, $\dot{\varepsilon}_y = \dot{\varepsilon}$, and thus θ comes out to be –1.0 (total strain reversal).

Following the same analysis, for ECAP followed by plane-strain compression with Z being the loading direction, X is the rolling direction, and Y is the transverse direction, θ comes out to be 0.5 which is half way between monotonic and orthogonal loading (for ZND $\rightarrow \dot{\varepsilon}_z = -\dot{\varepsilon}$, $\dot{\varepsilon}_x = \dot{\varepsilon}$, $\dot{\varepsilon}_y = 0$). Strain path can vary from monotonic loading, where $\theta = 1.0$, to orthogonal loading, which is characterized by a high level of severity in the deformation sequence, where $\theta = 0$, to complete reversal straining, which is

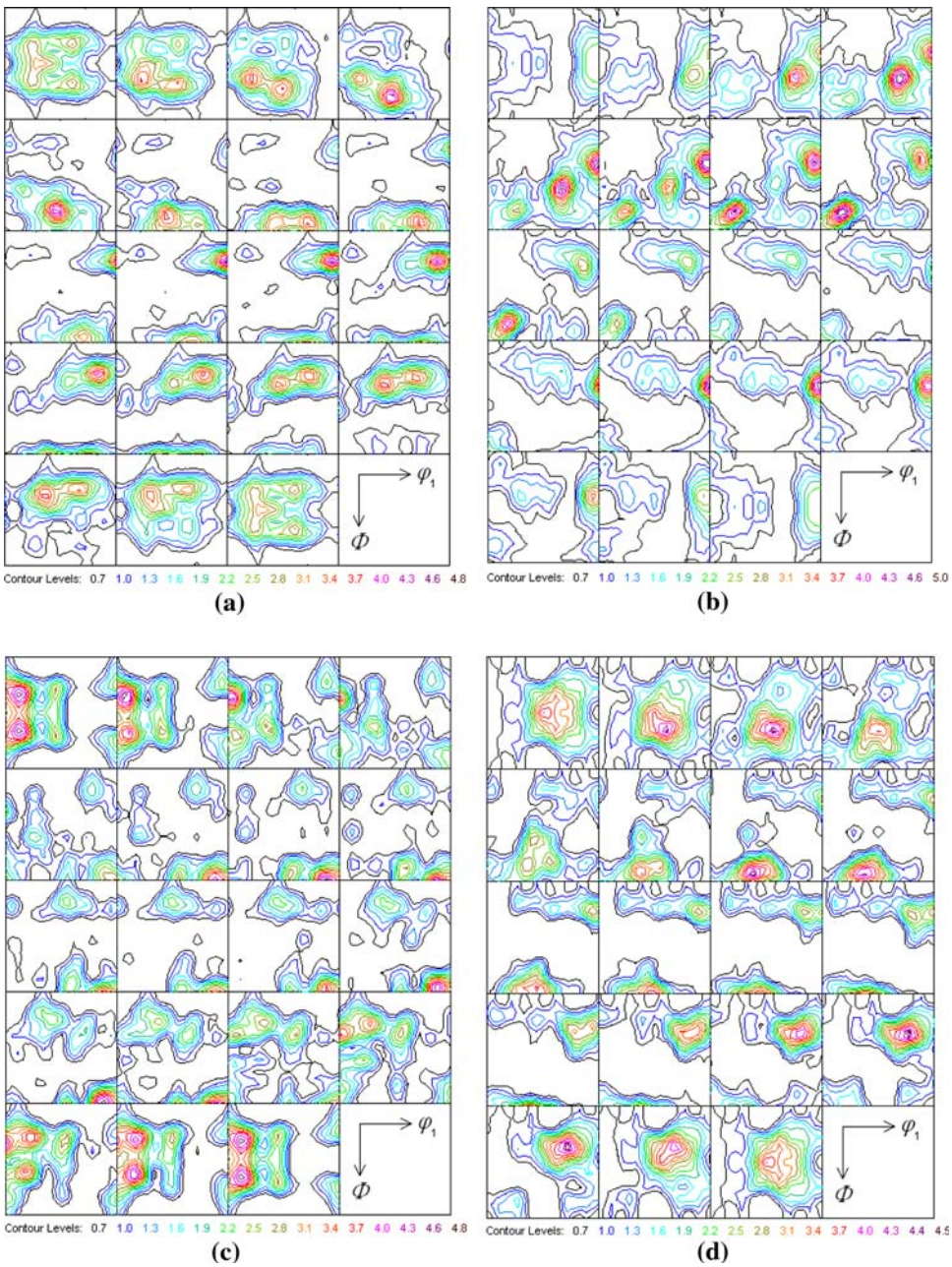

Fig. 4 Orientation distribution function plots for constant ϕ_2 sections of samples ECAP processed to four passes and plane strain compressed to a true axial strain of 0.5, via XND (**a**) and ZND (**b**). XND (**c**) and ZND (**d**) are for the same ECAP condition, but the plane strain compression was to a true axial strain of 1.0

characterized by softening due to the Bauschinger effect, where $\theta = -1.0$. Thus, the calculated values can account for the higher flow stresses in ZND.

Texture evolution

Texture measurements were performed on samples ECAP processed to one, two, and four passes, via route B_c, and then plane strain compressed in XND and ZND to two true axial strain levels of 0.5 and 1.0. Texture was measured on the RD–TD plane of the plane-strain-compressed samples. Figure 3a, b represents the (100), (110), and (111) pole figures for the samples ECAP processed to four passes and then plane strain compressed to a true axial strain of 0.5 in the XND and ZND directions, respectively. Figure 3c, d is for the same ECAP condition, but plane-strain compression was to a true axial strain of 1.0. Figure 4 represents the ODF plots with constant ϕ_2 sections, calculated for the conditions stipulated in Fig. 3. In order to save space, the pole figures and ODF plots for other samples are not shown here. However, the intensities of the texture orientations are presented in the next paragraph. The purpose of this texture documentation is to compare the texture evolution (spatial distribution of orientations and their intensities) after plane-strain compression with totally different initial textures arising from the different cutting procedure of the ECAPed samples, and the different textures that evolve with ECAP number of passes. It is reported that texture evolves differently with the number of ECAP passes [17], due to the successive change of the shearing plane associated with rotating the sample between subsequent pressings. The main ideal orientations that reflect the rolling textures in fcc metals, and considered in this study, can be seen in Table 1.

Figure 5a represents the f(g) as depicted from the ODF plots for the main ideal orientations that reflect the rolling texture for samples that were ECAP processed to one pass and then plane strain compressed in XND and ZND to a true axial strain of 0.5. Figure 5b, c represents same

Table 1 The main ideal orientations of rolling texture in fcc metals considered in this study

Notation	Miller index $\{hkl\}\ \langle uvw\rangle$	Euler angles (°)		
		ϕ_1	ϕ	ϕ_2
T	$\{444\}\ \langle 11\,11\,\bar{8}\rangle$	90	27	45
Cu	$\{112\}\ \langle 11\bar{1}\rangle$	90	35	45
B	$\{011\}\ \langle 21\bar{1}\rangle$	35	45	0
S_1	$\{124\}\ \langle 21\bar{1}\rangle$	57	29	63
S_2	$\{123\}\ \langle 41\bar{2}\rangle$	47	37	63
S_3	$\{123\}\ \langle 63\bar{4}\rangle$	59	37	63
G	$\{011\}\ \langle 100\rangle$	0	45	0

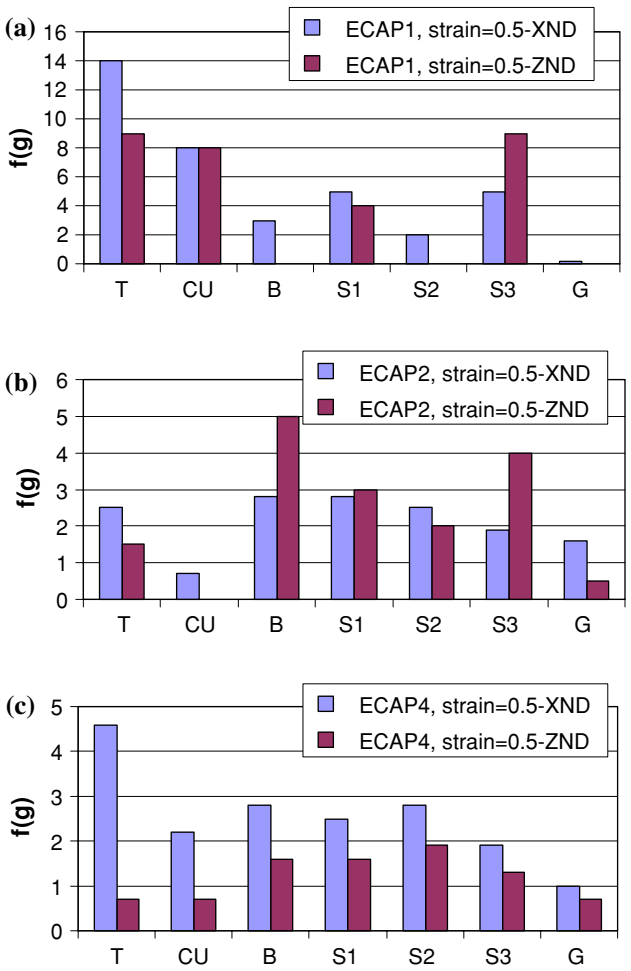

Fig. 5 f(g) values of ideal orientations in rolling texture for samples ECAP processed to one (**a**), two (**b**), and four (**c**) passes, and plane strain compressed to a strain of 0.5 loaded in two different directions, XND and ZND

information but for samples pre-ECAP processed to two and four passes. It is concluded, from the measured pole figures, that in both cases (XND and ZND) the texture exhibits a clear transition to capture the features of the rolling texture even though the starting texture is totally different in each case. Figure 5 shows, clearly, that the two deformation paths develop different intensities for the main ideal rolling-texture components. Thus, manipulating the deformation paths can be an effective technique for tailoring the rolling texture.

To document the evolution of texture in these two deformation paths (ECAP → XND, ECAP → ZND), ECAP processed samples were plane-strain compressed to a true axial strain of 1.0. Figure 6a, b, and c represents the evolution of texture for samples ECAP processed to one, two, and four passes, respectively, and then plane strain compressed in ZND. Figure 6d–f is for XND. The summation of the T and Cu orientations gives an indication to

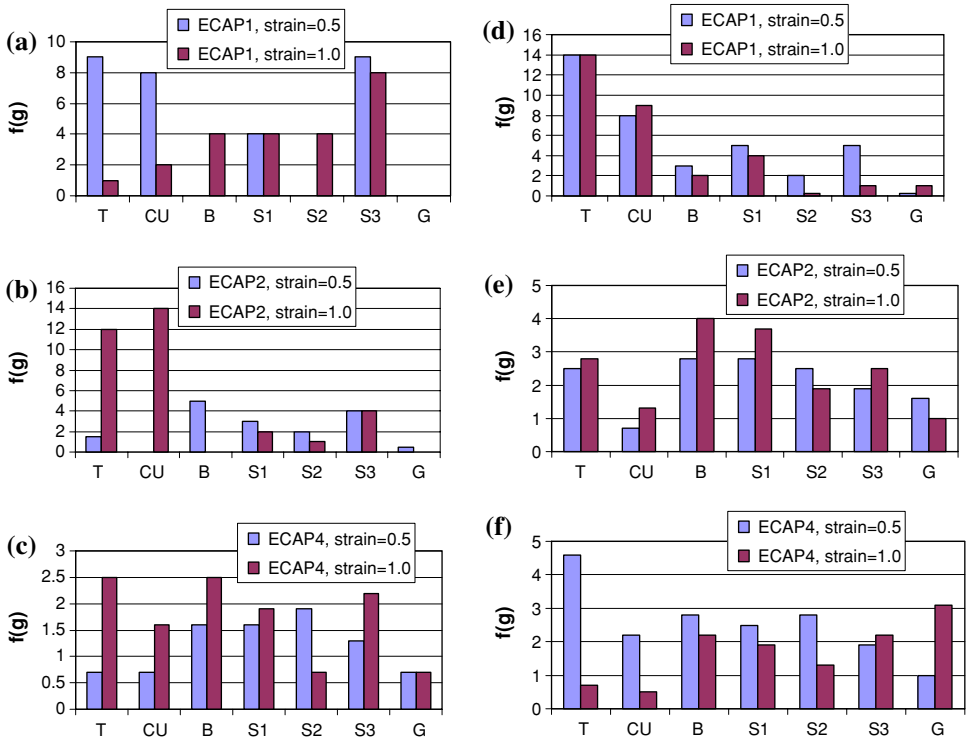

Fig. 6 **a**, **b**, and **c** represent the f(g) values for the ideal rolling-texture components for samples plane strain compressed in ZND, for two strain levels of 0.5 and 1.0, for samples ECAP processed to one, two, and four passes, respectively. **d**–**f** represent same information but for XND

the rise of a copper-type texture, whereas the B orientation is a texture component that gives rise to a brass-type texture. It can be seen that, for ZND, for samples ECAP processed to one pass, the copper-type texture initially dominates at a strain of 0.5, whereas at the higher strain both copper and brass components almost equally coexist. For samples ECAP processed to two passes, the brass component initially dominates and at a strain of 1.0 the copper-type texture components become extremely strong with the disappearance of the B component. For samples ECAPed to four passes, the copper components almost equally coexist with the brass component at both strain levels. For XND, for samples ECAP processed to one pass, the copper-type texture totally dominates, for the two deformation levels investigated. For samples ECAP processed to two passes, the copper- and brass-type texture evolves in an almost equal fashion. For samples ECAP processed to four passes, at a strain of 0.5, the copper-type texture dominates, while at a strain of 1.0 the brass-type texture component is slightly higher. This ascertains that the initial texture can influence the way rolling texture develops in plane strain and to large strains. Worth mentioning is that the intensity of these texture distributions could be affected by changing the pressing speed in plane-strain compression due to the change of dynamic recovery rates as suggested in the process of ECAP [5]. The annealing texture of such new tailored texture distributions could be of major industrial significance. This point is under current study and is motivated by the fact that deep drawing properties of aluminum is determined by the relative proportions of the cube and retained rolling-texture components. Other researchers [18] have attempted manipulating the strength of the annealing texture by investigating the effect of homogenization treatment before cold rolling of Al–Fe–Si alloy.

Conclusions

Combining ECAP with plane-strain compression and also with changing the loading direction will produce well-known rolling textures, but with different texture component intensities. This can provide an effective tool for tailoring the rolling texture. ZND processing always gave higher flow stresses and this path was characterized to be half way between monotonic and orthogonal loading, while for XND the strain path was characterized by total strain reversal which can lead to softening because of the Bauschinger effect.

Acknowledgement The Center of Excellence for Research in Engineering Materials (CEREM) is greatly acknowledged for the support of this research.

References

1. El-Danaf EA (2008) Mater Sci Eng A 487:189
2. Iwahashi Y, Wang J, Horita Z, Nemoto M, Langdon TG (1996) Scripta Mater 35:143
3. Zhilyaev AP, Lee S, Nurislamova GV, Valiev RZ, Langdon TG (2001) Scripta Mater 44:2753
4. Huang Y, Prangnell PB (2008) J Mater Sci 43:7273. doi: 10.1007/s10853-008-2623-0
5. Berbon PB, Furukawa M, Horita Z, Nemoto M, Langdon TG (1999) Met Trans A 30A:1989
6. Iwahashi Y, Horita Z, Nemoto M, Langdon TG (1998) Acta Mater 46:3317
7. Martins JP, Carvalho ALM, Padilha AF (2009) J Mater Sci 44:2966. doi:10.1007/s10853-009-3393-z
8. Saiyi L, Beyerlein IJ, Alexander DJ, Vogel SC (2005) Scripta Mater 52:1099
9. Saiyi L, Kalidindi SR, Beyerlein J (2005) Mater Sci Eng A 410–411:207
10. Saiyi L, Beyerlein J, Alexander DJ, Vogel SC (2005) ActaMater 53:2111
11. Hoseini M, Meratian M, Li H, Szpunar JA (2008) J Mater Sci 43:4561. doi:10.1007/s10853-008-2638-6
12. Hirsch J, Lucke K (1988) Acta Metall 36:2863
13. Leffers T, Ray RK (2009) Prog Mater Sci 54:351
14. Terada D, Houda H, Tsuji N (2008) J Mater Sci 43:7331. doi: 10.1007/s10853-008-2809-5
15. Schmitt J, Aernoudt E, Baudelet B (1985) Mater Sci Eng 75:13
16. Saiyi L (2007) Scripta Mater 56:445
17. El-Danaf EA (2008) Mater Sci Eng A 492:141
18. Birol Y (2008) J Mater Sci 43:4652.doi:10.1007/s10853-008-2663-5